Journal of Alloys and Compounds 506 (2010) 868–871

Contents lists available at ScienceDirect

Journal of Alloys and Compounds

journal homepage: www.elsevier.com/locate/jallcom

Influence of MoO_3 doping on structure and electrical conductivity of defect fluorite-type $Gd_2Zr_2O_7$

Zhan-Guo Liu, Shuai Gao, Jia-Hu Ouyang*, Xiao-Liang Xia

Institute for Advanced Ceramics, Department of Materials Science, Harbin Institute of Technology, No. 92 West Da-Zhi Street, Harbin 150001, China

ARTICLE INFO

Article history:
Received 8 June 2010
Received in revised form 8 July 2010
Accepted 10 July 2010
Available online 17 July 2010

Keywords:
$Gd_2(Zr_{1-x}Mo_x)_2O_{7+2x}$
Electrolyte
Impedance spectroscopy
Electrical conductivity

ABSTRACT

In this paper, we report the preparation, structure and electrical conductivity of MoO_3-doped zirconates with a nominal chemical formula of $Gd_2(Zr_{1-x}Mo_x)_2O_{7+2x}$ ($x = 0, 0.1, 0.2$). X-ray diffraction measurements indicate that $Gd_2Zr_2O_7$ exhibits a defect fluorite-type structure, and $Gd_2(Zr_{1-x}Mo_x)_2O_{7+2x}$ ($x = 0.1, 0.2$) have a single phase of pyrochlore-type structure. The alternating current (AC) impedance measurements show that the electrical conductivity of $Gd_2(Zr_{1-x}Nb_x)_2O_{7+2x}$ ceramics obeys the Arrhenius equation, and gradually increases with increasing temperature from 673 to 1173 K. The activation energy and pre-exponential factor for electrical conductivity gradually decrease with the increase of MoO_3 content. $Gd_2(Zr_{1-x}Mo_x)_2O_{7+2x}$ ceramics are oxide-ion conductors in the oxygen partial pressure range of 1.0×10^{-4} to 1.0 atm at all test temperature levels. The electrical conductivity of defect fluorite-type $Gd_2Zr_2O_7$ is not improved by MoO_3 doping.

1. Introduction

Solid oxide fuel cells (SOFCs) are generally considered as a clean, efficient and silent technology with a variety of potential applications [1]. Typically, SOFCs consist of an ionic conducting electrolyte and mixed ionic and electronic conducting electrodes (cathode and anode). The conventional electrolyte is 8 mol% Y_2O_3–ZrO_2 (YSZ), and the anode is Ni–YSZ cermets and cathode is $La_{1-x}Sr_xMnO_3$ oxide, respectively [2–4]. However, unwanted chemical reactions generally take place at the cathode/electrolyte interface when SOFCs are operated at high temperatures for a long time. It will generate insulating $La_2Zr_2O_7$ and $SrZrO_3$ at the interface, which may have a detrimental effect on SOFCs performance [5,6]. In last several decades, great efforts can be found on improving the electrical conductivity of solid electrolytes [7–9]. It is well known that the electrical conductivity of solid electrolytes is affected by a lot of factors such as microstructure, ionic radius and valence of doping elements, and oxygen vacancy concentration, etc. [10–12]. There is a great deal of interest in the reducing the operating temperature of SOFCs. Complex oxides with the $A_2B_2O_7$-type structure, where A is a trivalent rare-earth element and B represents a tetravalent transition metal element, show an excellent electrical properties owing to high compositional diversity, structural flexibility and intrinsic concentration of oxygen vacancies [13,14]. van Dijk et al. [15,16] prepared $Gd_xZr_{1-x}O_{2-x/2}$ ($0.2 < x < 0.6$) ceramics, and found that the stoichiometric $Gd_2Zr_2O_7$ had a maximum in ionic conductivity and a minimum in activation energy at temperatures between 773 and 1023 K. $Gd_2Zr_2O_7$ ceramics doped with different cations at A sites were widely investigated as potential solid electrolytes for SOFCs [17–22]. $Gd_2Zr_2O_7$ doped with 5 and 10 mol% Sr showed a higher electrical conductivity than undoped $Gd_2Zr_2O_7$ in the temperature range of 773–973 K [17]. A significant increase in electrical conductivity was found by suitable substitution of Sm or Nd at the Gd site in $Gd_2Zr_2O_7$ ceramic [18,19]. However, the electrical conductivity of $(Gd_{1-x}La_x)Zr_2O_7$ ($0 \le x \le 1.0$) ceramics was almost La-content independent from 773 to 1023 K [5,6]. For $(Gd_{1-x}Yb_x)_2Zr_2O_7$ ($0 \le x \le 1.0$) ceramics, the electrical conductivity gradually decreases with the increase of Yb content at identical temperature levels [20]. Moon and Tuller [21] found that $Gd_2(Zr_{0.9}Ti_{0.1})_2O_7$ had the highest electrical conductivity in $Gd_2(Zr_{1-x}Ti_x)_2O_7$ ($0 \le x \le 1.0$) ceramics, and the electrical conductivity was comparable to YSZ at identical temperature levels.

To the best of our knowledge, there is no report on structure and electrical conductivity of MoO_3-doped $Gd_2Zr_2O_7$ in the open literatures. It is interesting to study the influence of the substitution of hexavalent Mo at the Zr site on the structure and electrical conductivity of $Gd_2Zr_2O_7$ ceramic. In this work, the preparation, structure and electrical conductivity of $Gd_2(Zr_{1-x}Mo_x)_2O_{7+2x}$ ($x = 0, 0.1, 0.2$) ceramics were investigated in detail.

2. Experimental

Zirconate ceramics with a nominal chemical formula of $Gd_2(Zr_{1-x}Mo_x)_2O_{7+2x}$ ($x = 0, 0.1, 0.2$) were prepared by a conventional solid-state reaction method in

* Corresponding author. Tel.: +86 451 86414291; fax: +86 451 86414291.
E-mail address: ouyangjh@hit.edu.cn (J.-H. Ouyang).

0925-8388/$ – see front matter © 2010 Elsevier B.V. All rights reserved.
doi:10.1016/j.jallcom.2010.07.101

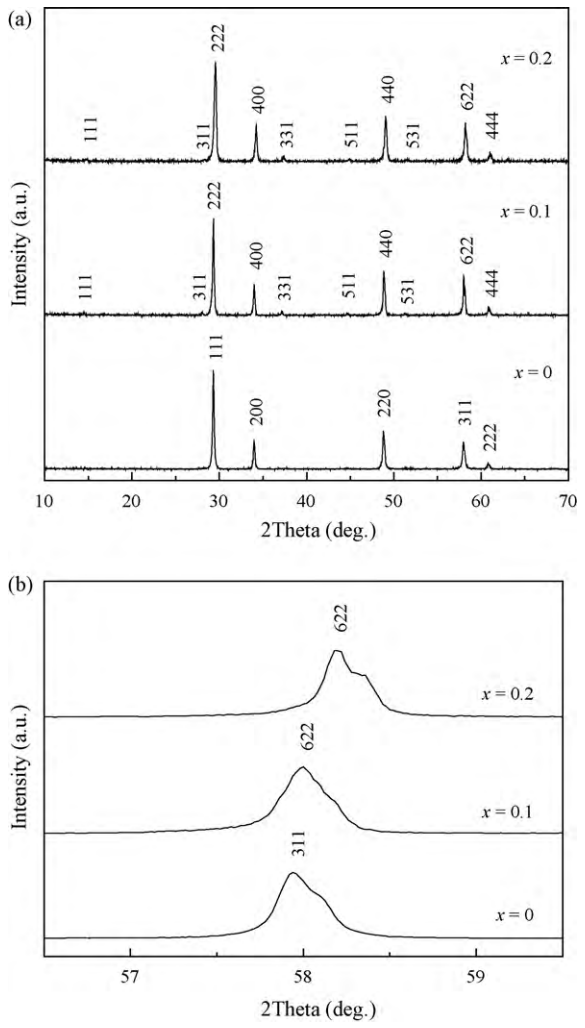

Fig. 1. XRD patterns of $Gd_2(Zr_{1-x}Mo_x)_2O_{7+2x}$ ceramics sintered at 1973 K for 10 h in air: (a) in 2θ range of 10–70°; (b) $(3\,1\,1)_F/(6\,2\,2)_{Py}$ peak in 2θ range of 56.5–59.5°.

air using stoichiometric amounts of Gd_2O_3 (Grirem Advanced Materials Co. Ltd., China; purity ≥ 99.99%), ZrO_2 (Dongguan SG Ceramics Technology Co. Ltd., China; purity ≥ 99.9%) and MoO_3 (Shanghai Colloid Chemical Plant, China; purity ≥ 99.5%). The powders were mechanically mixed for 24 h at rotating speed of 300 rpm using zirconia ball and absolute ethyl alcohol as milling media. The mixed powders were dried and then pressed into pellets using a uniaxial stress. Subsequently, the pellets were further compacted by an isostatic pressure of 280 MPa for 5 min. The pressed pellets were pressureless-sintered at 1973 K for 10 h in air. The densities of sintered samples were measured by the Archimedes principle with an immersion medium of deionized water. The phase structure of sintered samples was characterized by an X-ray diffractometer (Rigaku D/Max 2200VPC, Japan) with Cu Kα radiation at a scan rate of 4°/min. A step scan procedure (0.02°/2θ step, time per step 3 s) on the diffraction peaks of $(3\,1\,1)_F/(6\,2\,2)_{Py}$ was recorded to determine the evolution of X-ray spectrum.

The impedance measurements were performed on sintered pellets (~1 mm in thickness, ~8 mm in diameter) in air using platinum electrodes. Platinum paste was applied on both sides of the sintered pellets, and cured at 1223 K for 2 h in air to remove the organic binders. The alternating current (AC) impedance spectra were obtained using an impedance/gain-phase analyzer (Solartron™ SI 1260, UK). Impedance measurements were conducted on heating from 673 to 1173 K in a frequency range from 2 MHz to 200 Hz with an increment interval of 50 K. The impedance spectra were also measured in an oxygen partial pressure $p(O_2)$ range of 1.0×10^{-4} to 1.0 atm. Software equivalent circuit Zview 3.1c was used to analyze the AC impedance data.

3. Results and discussion

Fig. 1 shows the XRD patterns of $Gd_2(Zr_{1-x}Mo_x)_2O_{7+2x}$ ceramics sintered at 1973 K for 10 h in air. From Fig. 1(a), $Gd_2Zr_2O_7$ ceramic exhibits a defect fluorite-type structure, and $Gd_2(Zr_{1-x}Mo_x)_2O_{7+2x}$ ($x = 0.1$, 0.2) ceramics have a pyrochlore-type structure, which is characterized by the presence of typical superstructure diffraction peaks at the 2θ values of about 14° (1 1 1), 28° (3 1 1), 37° (3 3 1), 45° (5 1 1) and 51° (5 3 1) using Cu Kα radiation [22–24]. No other phases are identified from Fig. 1(a). The XRD patterns of $(3\,1\,1)_F/(6\,2\,2)_{Py}$ peak for $Gd_2(Zr_{1-x}Mo_x)_2O_{7+2x}$ ceramics are shown in Fig. 1(b), which indicates that these peaks gradually shift to the high angle region with the increase of MoO_3 content. The MoO_3-doped $Gd_2Zr_2O_7$ can be simply expressed using the defect equilibrium reaction as:

$$MoO_3 \xrightarrow{Gd_2Zr_2O_7} Mo_{Zr}^{\bullet\bullet} + O_i'' + 2O_O \quad (1)$$

where $Mo_{Zr}^{\bullet\bullet}$, O_i'' and $2O_o$ represent a hexavalent Mo cation at a tetravalent Zr cation site, an oxygen anion at the interstitial site and two oxygen anions on regular oxygen anion sites in the crystal structure, respectively.

In the $A_2B_2O_7$ system, the phase structure is mainly governed by the ionic radius ratio of $r(A^{3+})/r(B^{4+})$. The stability of pyrochlore-type structure in zirconates is limited to the range of $1.46 \le r(A^{3+})/r(B^{4+}) \le 1.78$ at an atmospheric pressure [14]. The ionic radius of Gd^{3+} is 0.1053 nm in eightfold coordination, and the ionic radius of Zr^{4+} and Mo^{6+} is 0.072 and 0.059 nm in the sixfold coordination, respectively [25]. The value of $r(A^{3+})/r(B^{4+})$ is equal to 1.46 for $Gd_2Zr_2O_7$, and $Gd_2Zr_2O_7$ shows a defect fluorite-type structure owing to high sintering temperature of 1973 K used in this work, which is higher than the phase transition temperature (1803 K) of $Gd_2Zr_2O_7$ [26]. For $Gd_2(Zr_{1-x}Mo_x)_2O_{7+2x}$ ($x = 0.1$, 0.2) ceramics in this work, the values of $r(A^{3+})/r(B^{4+})$ are clearly larger than 1.46 since the ionic radius of Mo^{6+} is smaller than that of Zr^{4+}, and therefore $Gd_2(Zr_{1-x}Mo_x)_2O_{7+2x}$ ($x = 0.1$, 0.2) ceramics exhibit a pyrochlore-type structure. Table 1 presents the relative densities of $Gd_2(Zr_{1-x}Mo_x)_2O_{7+2x}$ ceramics sintered at 1973 K for 10 h in air. It shows that $Gd_2(Zr_{1-x}Mo_x)_2O_{7+2x}$ ceramics have a high relative density of 96.0–97.3%.

Table 1
Relative densities of $Gd_2(Zr_{1-x}Mo_x)_2O_{7+2x}$ ceramics sintered at 1973 K for 10 h in air.

Ceramic materials	Relative density (%)
$Gd_2Zr_2O_7$	97.3
$Gd_2(Zr_{0.9}Mo_{0.1})_2O_{7.2}$	96.5
$Gd_2(Zr_{0.8}Mo_{0.2})_2O_{7.4}$	96.0

Fig. 2 shows typical impedance plots of $Gd_2(Zr_{1-x}Mo_x)_2O_{7+2x}$ ceramics at 723 K in air. The contributions due to grain and grain-boundary effects are obviously observed at high and low-frequency regions. In the ideal case, the frequency response of electrical conductivity of polycrystalline electrolytes can be modeled by a resistor–capacitor (RC) pair in parallel. However, in the present case, in place of capacitor a constant phase element (CPE) is required to model the experimental data [27], as shown in Fig. 2, respectively. From fitted results, for $Gd_2(Zr_{1-x}Mo_x)_2O_{7+2x}$ ($x = 0$, 0.1, 0.2) ceramics, the capacitance for the high-frequency semicircles at 723 K in air is determined to be 2.08×10^{-10} F cm^{-1}, 2.85×10^{-10} F cm^{-1} and 3.17×10^{-10} F cm^{-1}, respectively, while the low-frequency semicircles show capacitance at 723 K in air is 5.04×10^{-7} F cm^{-1}, 1.02×10^{-7} F cm^{-1}, and 6.91×10^{-8} F cm^{-1}, respectively. These values are typical for the grain and grain-boundary contributions in solid electrolyte materials. The electrical resistance value of each composition of $Gd_2(Zr_{1-x}Mo_x)_2O_{7+2x}$ ceramics, R, is determined from the intercept of the corresponding low-frequency semicircle on the Z' axe [27]. The electrical conductivities of $Gd_2(Zr_{1-x}Mo_x)_2O_{7+2x}$ ceramics are calculated from the values of resistance at corresponding temperatures and the geometrical dimensions of the measured samples.

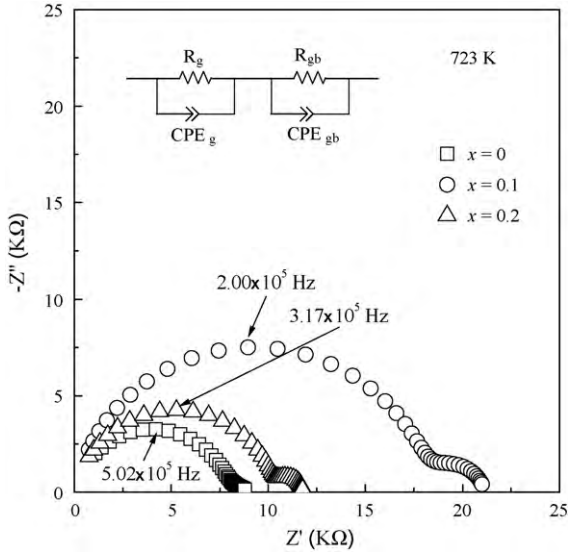

Fig. 2. Typical AC impedance plots and corresponding equivalent circuit of $Gd_2(Zr_{1-x}Mo_x)_2O_{7+2x}$ ceramics ($x = 0$, 0.1, 0.2) at 723 K in air. R_g, R_{gb}, CPE_g and CPE_{gb} represent grain resistance, grain-boundary resistance, constant phase element of the grain and constant phase element of the grain-boundary.

The temperature dependence of electrical conductivity could be plotted based on the Arrhenius equation with the following expression:

$$\sigma \cdot T = \sigma_0 \exp(-E/k_B T) \quad (2)$$

where σ, T, σ_0, E and k_B are electrical conductivity, absolute temperature, pre-exponential factor, activation energy and Boltzman constant, respectively. Fig. 3 shows the Arrhenius plots for electrical conductivity of $Gd_2(Zr_{1-x}Mo_x)_2O_{7+2x}$ ceramics in air. The electrical conductivity data follow the approximately linear behavior, which confirms that the ionic diffusion process is thermally activated. The activation energy and pre-exponential factor of $Gd_2(Zr_{1-x}Mo_x)_2O_{7+2x}$ ceramics are calculated from the slope and the intercept of the linear fits in the Arrhenius plots (Fig. 3), respectively, as shown in Table 2. Clearly, both activation energy and pre-exponential factor of $Gd_2(Zr_{1-x}Mo_x)_2O_{7+2x}$ ceramics gradually decrease with the increase of MoO_3 content.

Fig. 4 shows the electrical conductivity of $Gd_2(Zr_{1-x}Mo_x)_2O_{7+2x}$ ceramics as a function of MoO_3 content at different temperatures. Clearly, electrical conductivity of $Gd_2(Zr_{1-x}Mo_x)_2O_{7+2x}$ ceramics gradually increases with increasing temperature from 673 to 1173 K. From Fig. 4, the electrical conductivity of $Gd_2(Zr_{1-x}Mo_x)_2O_{7+2x}$ ($x = 0.1$, 0.2) ceramics is lower than that of $Gd_2Zr_2O_7$, which indicates that the electrical conductivity of defect fluorite-type $Gd_2Zr_2O_7$ is not improved by MoO_3 doping. In the $A_2B_2O_7$-type structure, 7/8 anion sites are occupied by oxide-ions, and 1/8 anion sites are oxygen vacancy [14]. As shown in the defect equilibrium reaction (1), the doping of MoO_3 in $Gd_2Zr_2O_7$ leads to the decrease of the oxygen vacancy in $Gd_2Zr_2O_7$, which reduces the value of pre-exponential factor subsequently. The decrease in pre-exponential factor would lead to a decrease in electrical conductivity; however, the decrease in activation energy would promote the oxide-ion migration. Thus, these two processes are competing. As the MoO_3 content increases from 0 to 0.1, both pre-exponential factor and activation energy decrease as shown in Table 1. From Fig. 4, the electrical conductivity decreases from $x = 0$ to $x = 0.1$, which indicates that the decrease in activation energy is not able to compensate for the decrease in pre-exponential factor. From $x = 0.1$ to $x = 0.2$, both pre-exponential factor and activation energy continue to decrease, as shown in Table 1. However, the electrical conductivity increases from $x = 0.1$ to $x = 0.2$, which indicates that the decrease in activation energy can compensate for the decrease in pre-exponential factor, and finally causes the slight increase in electrical conductivity.

In practice, solid electrolytes should be purely ionic conductors at different oxygen partial pressures. Therefore, it is important to study the electrical conductivity of solid electrolytes at different oxygen partial pressures. The oxygen partial pressure $p(O_2)$ dependence of electrical conductivity was measured for $Gd_2(Zr_{1-x}Mo_x)_2O_{7+2x}$ ceramics in order to clarify conduction carrier. Fig. 5 shows the electrical conductivity of $Gd_2(Zr_{0.9}Mo_{0.1})_2O_{7.2}$ composition as a function of oxygen partial pressure at different temperatures. It is clearly seen that electrical conductivity of $Gd_2(Zr_{0.9}Mo_{0.1})_2O_{7.2}$ composition is almost independent of oxygen partial pressure from 1.0×10^{-4} to 1.0 atm at all test temperature

Table 2
Activation energy and pre-exponential factor of $Gd_2(Zr_{1-x}Mo_x)_2O_{7+2x}$ ceramics in air.

Ceramic materials	Activation energy E (eV)	Pre-exponential factor σ_0 (S cm^{-1} K)
$Gd_2Zr_2O_7$	1.09	7.43×10^5
$Gd_2(Zr_{0.9}Mo_{0.1})_2O_{7.2}$	0.99	5.09×10^4
$Gd_2(Zr_{0.8}Mo_{0.2})_2O_{7.4}$	0.93	3.93×10^4

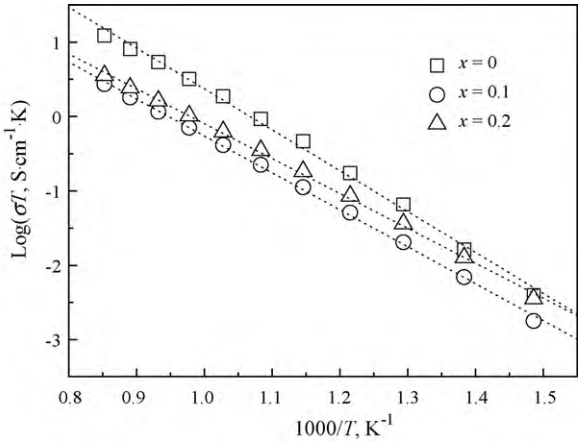

Fig. 3. Arrhenius plots for electrical conductivity of $Gd_2(Zr_{1-x}Mo_x)_2O_{7+2x}$ ceramics in air.

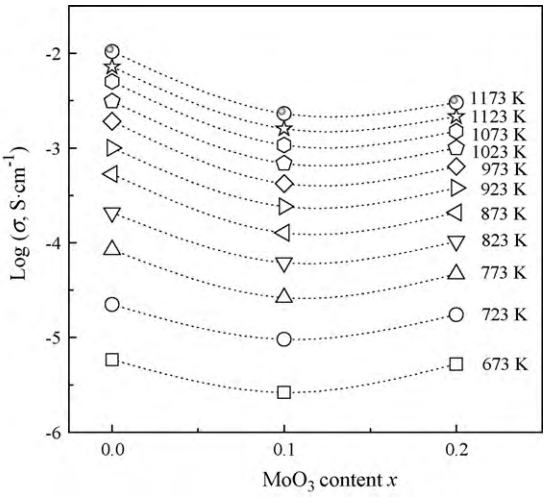

Fig. 4. Compositional dependence of electrical conductivity of $Gd_2(Zr_{1-x}Mo_x)_2O_{7+2x}$ ceramics in air.

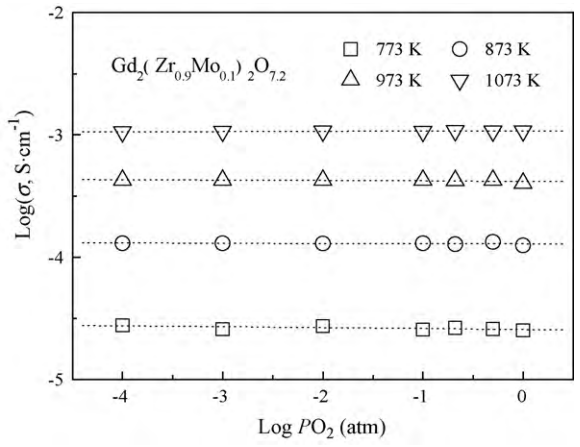

Fig. 5. Oxygen partial pressure dependence of electrical conductivity of the $Gd_2(Zr_{0.9}Mo_{0.1})_2O_{7.2}$ composition.

levels, which indicates that the conduction is purely ionic conductivity with negligible electronic conduction.

4. Conclusions

$Gd_2(Zr_{1-x}Mo_x)_2O_{7+2x}$ ($x = 0.1$, 0.2) have a single phase of pyrochlore-type structure, while $Gd_2Zr_2O_7$ exhibits a defect fluorite-type structure. The electrical conductivity of $Gd_2(Zr_{1-x}Mo_x)_2O_{7+2x}$ ceramics gradually increases with increasing temperature from 673 to 1173 K. The activation energy and pre-exponential factor of $Gd_2(Zr_{1-x}Mo_x)_2O_{7+2x}$ ceramics for electrical conductivity gradually decrease with the increase of MoO_3 content. $Gd_2(Zr_{1-x}Mo_x)_2O_{7+2x}$ ceramics are oxide-ion conductors in the oxygen partial pressure range of 1.0×10^{-4} to 1.0 atm at all test temperature levels. The electrical conductivity of defect fluorite-type $Gd_2Zr_2O_7$ is not improved by MoO_3 doping.

Acknowledgement

The authors would like to thank financial support from the National Natural Science Foundation of China (NSFC-No. 50972030).

References

[1] F. de Bruijn, Green Chem. 7 (2005) 132–150.
[2] W. Araki, Y. Imai, T. Adachi, J. Eur. Ceram. Soc. 29 (2009) 2275–2279.
[3] T.S. Li, W.G. Wang, H. Miao, T. Chen, C. Xu, J. Alloys Compd. 495 (2010) 138–143.
[4] M.C. Tucker, J. Power Sources 195 (2010) 4570–4582.
[5] J.A. Díaz-Guillén, M.R. Díaz-Guillén, K.P. Padmasree, A.F. Fuentes, J. Santamaría, C. León, Solid State Ionics 179 (2008) 2160–2164.
[6] J.A. Díaz-Guillén, A.F. Fuentes, M.R. Díaz-Guillén, J.M. Almanza, J. Santamaría, C. León, J. Power Sources 186 (2009) 349–352.
[7] S.J. Litzelman, J.L. Hertz, W. Jung, H.L. Tuller, Fuel Cells 8 (2008) 294–302.
[8] Y. Zheng, L. Wu, H. Gu, L. Gao, H. Chen, L. Guo, J. Alloys Compd. 486 (2009) 586–589.
[9] D. Maeland, C. Suciu, I. Waernhus, A.C. Hoffmann, J. Eur. Ceram. Soc. 29 (2009) 2537–2547.
[10] M. Mogensen, D. Lybye, N. Bonanos, P.V. Hendriksen, F.W. Poulsen, Solid State Ionics 174 (2004) 279–286.
[11] S. Hui, J. Roller, S. Yick, X. Zhang, C. Decès-Petit, Y. Xie, R. Maric, D. Ghosh, J. Power Sources 172 (2007) 493–502.
[12] A. Chroneos, R.V. Vovk, I.L. Goulatis, L.I. Goulatis, J. Alloys Compd. 494 (2010) 190–195.
[13] R.A. McCauley, J. Appl. Phys. 51 (1980) 290–294.
[14] M.A. Subramanian, G. Aravamudan, G.V. Subba Rao, Prog. Solid State Chem. 15 (1983) 55–143.
[15] T. van Dijk, K.J. de Vries, A.J. Burggraaf, Phys. Status Solidi A 58 (1980) 115–125.
[16] A.J. Burggraaf, T. van Dijk, M.J. Verkerk, Solid State Ionics 5 (1981) 519–522.
[17] K.V. Govindan Kutty, C.K. Mathews, T.N. Rao, U.V. Varadaraju, Solid State Ionics 80 (1995) 99–110.
[18] Z.-G. Liu, J.-H. Ouyang, Y. Zhou, X.-L. Xia, J. Power Sources 185 (2008) 876–880.
[19] B.P. Mandal, S.K. Deshpande, A.K. Tyagi, J. Mater. Res. 23 (2008) 911–916.
[20] Z.-G. Liu, J.-H. Ouyang, Y. Zhou, X.-L. Xia, J. Alloys Compd. 490 (2010) 277–281.
[21] P.K. Moon, H.L. Tuller, Solid State Ionics 28 (1988) 470–474.
[22] Z.-G. Liu, J.-H. Ouyang, Y. Zhou, J. Li, X.-L. Xia, J. Eur. Ceram. Soc. 29 (2009) 647–652.
[23] Z.-G. Liu, J.-H. Ouyang, Y. Zhou, M.-C. Meng, X.-L. Xia, Philos. Mag. 89 (2009) 553–564.
[24] Z.-G. Liu, J.-H. Ouyang, Y. Zhou, J. Alloys Compd. 472 (2009) 319–324.
[25] G.S. Rohrer, Structure and Bonding in Crystalline Materials, Cambridge University Press, Cambridge, 2004, pp. 521–525.
[26] D. Michel, M. Perez-y-Jorba, R. Collongues, Mater. Res. Bull. 9 (1974) 1457–1468.
[27] J.R. Macdonald, W.B. Johnson, in: E. Barsoukov, J.R. Macdonald (Eds.), Impedance Spectroscopy: Theory, Experiment and Applications, second ed., John Wiley & Sons, Inc., New Jersey, 2005 (Chapter 1).